Influence of elevated Nd fluxes on the northern Nd isotope end member of the Atlantic during the early Holocene

Frerk Pöppelmeier[1,2]*, Jeemijn Scheen[1], Patrick Blaser[2], Jörg Lippold[2], Marcus Gutjahr[3], Thomas F. Stocker[1]

[1]Climate and Environmental Physics, Physics Institute and Oeschger Centre for Climate Change Research, University of Bern, Bern, Switzerland

[2]Institute of Earth Sciences, Heidelberg University, Heidelberg, Germany

[3]GEOMAR Helmholtz Center for Ocean Research Kiel, Kiel, Germany

*Correspondence to: Frerk Pöppelmeier (frerk.poeppelmeier@climate.unibe.ch)

Contents of this file

Text S1: Bern3D model setup

The Bern3D model is based on a three-dimensional frictional-geostrophic ocean balance model (Edwards et al., 1998; Müller et al., 2006) with a Gent-McWilliams parameterization for eddy-induced transport (Griffies, 1998). The model is forced by monthly climatologies of NCEP/NCAR wind stress (Kalnay et al., 1996).

The biogeochemical module is described in detail in Parekh et al. (2008) and Tschumi et al. (2008). Production of particulate organic matter (POM), calcium carbonate ($CaCO_3$), and opal is limited to the euphotic zone defined as the uppermost 75 m and calculated as a function of light, phosphate, iron, and temperature (Figure 2; Doney et al., 2006). Below the euphotic zone all particles are globally uniformly remineralized, except dust which undergoes no remineralization in the water column. POM remineralizes following the description of Martin et al. (1987), while the remineralization of $CaCO_3$ and opal is described by exponential profiles with length-scales l_{CaCO3} = 2.9 km and l_{opal} = 10 km. Remaining particles in the bottommost grid cell are instantaneously remineralized.

Neodymium is implemented as two separated tracers: ^{143}Nd and ^{144}Nd with Nd_{tot} = ^{143}Nd + ^{144}Nd. The parametrization of the Nd sources follows Rempfer et al. (2011) with changes as described in the main text (section 2.1). The only sink of Nd in the ocean is reversible particle scavenging which is parametrized by the ratio of particulate to dissolved Nd concentration (see Table S2) as described in detail by Rempfer et al. (2011).

Table S1: Sediment core sites of compiled Nd isotope reconstructions covering the Holocene.

Site	Lat (°N)	Long (°E)	Depth (m)	Archive	Reference
BOFS 28K	24.6	-22.8	4900	foram	Howe et al. (2017)
BOFS 29K	20.6	-21.1	4000	foram	Howe et al. (2017)
BOFS 30K	19.0	-20.2	3580	foram	Howe et al. (2017)
BOFS 31K	19.0	-20.2	3300	foram	Howe et al. (2017)
BOFS 32K	22.5	-22.0	4500	foram	Howe et al. (2017)
GeoB 1523-1	3.8	-41.6	3292	foram	Lippold et al. (2016)
GeoB 2107-3	-27.2	-46.5	1048	leach	Howe et al. (2016a)
GeoB 3808-6	-30.8	-14.7	3213	foram	Jonkers et al. (2015)
IODP 1313	41.0	-33.0	3413	foram+leach	Howe et al. (2016b) Pöppelmeier et al. (2019)
KNR 198-35/36	40.0	-69.0	1820	foram	Zhao et al. (2019)
KNR159-5-30GGC	-28.1	-46.1	2500	leach	Pöppelmeier et al. (2020)
KNR159-5-33GGC	-27.6	-46.2	2082	leach	Pöppelmeier et al. (2020)
M35003-4	12.1	-61.2	1299	leach	Lippold et al. (2016)
M45-5 KL86	43.4	-22.5	3028	leach	This study
M45-5 KL90	31.6	-28.0	3143	leach	This study
M78/1-235	11.6	-61.0	852	foram	Poggemann et al. (2018)
MD02-2594	-43.7	17.3	2440	foram+fish +leach	Wei et al. (2016)
MD07-3076Q	-44.1	-14.2	3770	foram+fish	Skinner et al. (2013)
ODP 1056	32.5	-76.3	2167	leach	Pöppelmeier et al. (2019)
ODP 1059	31.7	-75.4	2985	leach	Pöppelmeier et al. (2019)
ODP 1089	-40.9	9.9	4621	leach	Lippold et al. (2016)
ODP 659	18.1	-21.0	3071	leach	This study
ODP 662	-1.4	-11.7	4035	leach	This study
ODP 664	0.1	-23.2	3806	leach	This study
ODP 925	4.2	-43.5	3040	foram	Howe et al. (2017)
ODP 928	5.5	-43.8	4012	foram	Howe et al. (2017)
ODP 929	6.0	-43.7	4360	foram	Howe et al. (2017)
SU90-03	40.5	-32.0	2475	foram	Howe et al. (2016b)

Table S2: Comparison of parameters and Nd flux contributions to the combined total Nd source between Rempfer et al. (2011; 2012) and this study for control simulations. Parameters in red are used for tuning in this study. Note that the benthic flux was called 'boundary source' in Rempfer et al. (2011; 2012).

		Rempfer et al. (2011)	Rempfer et al. (2012)	This study
Dust flux (g/m²/a)	f_{du}	Luo et al. (2003)	Luo et al. (2003)	Mahowald et al. (2006)
Particle settling velocity (m/a)		1000	1000	1000
Nd concentration dust (µg/g)	c_{du}	20	20	20
Nd release from dust (%)	β_{du}	2	2	2
εNd dust		Tachikawa et al. (2003)	Tachikawa et al. (2003)	Tachikawa et al. (2003)
Nd concentration rivers	c_{ri}	Goldstein and Jacobsen (1987)	Goldstein and Jacobsen (1987)	see main text
εNd rivers		Goldstein and Jacobsen (1987)	Goldstein and Jacobsen (1987)	see main text
Nd removal in estuaries (%)	γ	70	70	70
Riverine scaling	α_{ri}	1	1	3.5
Benthic flux depth limit (m)		3000	3000	5000 (max depth)
Benthic flux source		vertical surfaces	vertical surfaces	all surfaces
Benthic flux scaling	α_{bs}	1	1	variable (Fig. 3d)
[Nd]$_p$/[Nd]$_d$		0.001	0.0014	0.0014
Total benthic flux (g/a)	f_{bs}	5.5×10^9	4.5×10^9	3.3×10^9
Total riverine flux (g/a)	f_{ri}	0.34×10^9	0.34×10^9	1.77×10^9
Total dust flux (g/a)	f_{du}	0.26×10^9	0.26×10^9	0.50×10^9
Total flux (g/a)	f_{tot}	6.1×10^9	5.1×10^9	5.55×10^9
Residence time (a)	τ	700	720	690

Updated parametrization of the Nd-module:

The updated parametrization of the Nd-module closely follows Rempfer et al. (2011) but introduces new scaling factors. The equations for the Nd sources now read:

$$S_{du}(\theta,\phi) = F_{du}(\theta,\phi) \cdot c_{du} \cdot \beta_{du} \cdot \frac{1}{\Delta z_1} \tag{S1}$$

$$S_{ri}(\theta,\phi) = F_{ri}(\theta,\phi) \cdot c_{ri}(\theta,\phi) \cdot (1-\gamma) \cdot \frac{\alpha_{ri}}{V_{\theta,\phi}} \tag{S2}$$

$$S_{bs}(\theta,\phi,z) = f_{bs} \cdot \frac{A(\theta,\phi,z)}{A_{tot}} \cdot \frac{\alpha_{bs}(\theta,\phi)}{V_{\theta,\phi,z}} \tag{S3}$$

Here θ and ϕ correspond to the longitude and latitude, respectively. Δz_1 is the thickness of the uppermost grid cell (39 m), $V_{\theta,\phi,(z)}$ and $A_{\theta,\phi,z}$ are the volume and area at a given longitude, latitude, and depth. α_{ri} and $\alpha_{bs}(\theta,\phi)$ are the newly introduced scaling factors for the riverine and benthic Nd fluxes, respectively. Parameters and their values are listed in Table S2. The only sink of Nd in the Bern3D model, reversible scavenging, has not been changed from the implementation by Rempfer et al. (2011) (Eq. 10).

For the tuning of the updated Nd-module we varied f_{bs} between 1 and 5×10^9 g/a, $[Nd]_p/[Nd]_d$ between 0.0010 and 0.0016, and α_{ri} between 1.5 and 4.5 (Figure S4) and compared the results to the updated NEOSYMPA database. The MAEs of εNd and the Nd concentration are not minimized with the same set of parameters as was also reported by previous studies (Gu et al., 2019; Rempfer et al., 2011). MAE(εNd) is minimized with $f_{bs} = 4\times10^9$ g/a, $[Nd]_p/[Nd]_d = 0.0016$, and $\alpha_{ri} = 4.5$, while MAE($[Nd]_d$) is minimized with $f_{bs} = 2\times10^9$ g/a, $[Nd]_p/[Nd]_d = 0.0010$, and $\alpha_{ri} = 2.5$. To represent both εNd and $[Nd]_d$ reasonably well in the model, we choose $f_{bs} = 3.3\times10^9$ g/a, $[Nd]_p/[Nd]_d = 0.0014$, and $\alpha_{ri} = 3.5$ as a compromise (see Table S2).

Choice of the benthic Nd flux scaling (α_{bs}):

The regional elevated benthic Nd fluxes parameterized by the benthic Nd flux scaling (α_{bs}) of the control run were obtained by regional extrapolation of reported strong influences of a benthic source to the local bottom water (Abbott et al., 2015; Blaser et al., 2020; Grenier et al., 2013; Lacan and Jeandel, 2005; Rahlf et al., 2020; Wu, 2019). To test for the impact of regional elevated α_{bs} on the Nd isotopic distribution, we performed a simulation with α_{bs} globally set to 1 (Figure S1). Overall, the difference in the Atlantic εNd distributions between the control run and the one with $\alpha_{bs}(global) = 1$ is relatively small, with NADW being more radiogenic by slightly less than 0.5 ε-units and changes elsewhere tending towards less radiogenic signatures.
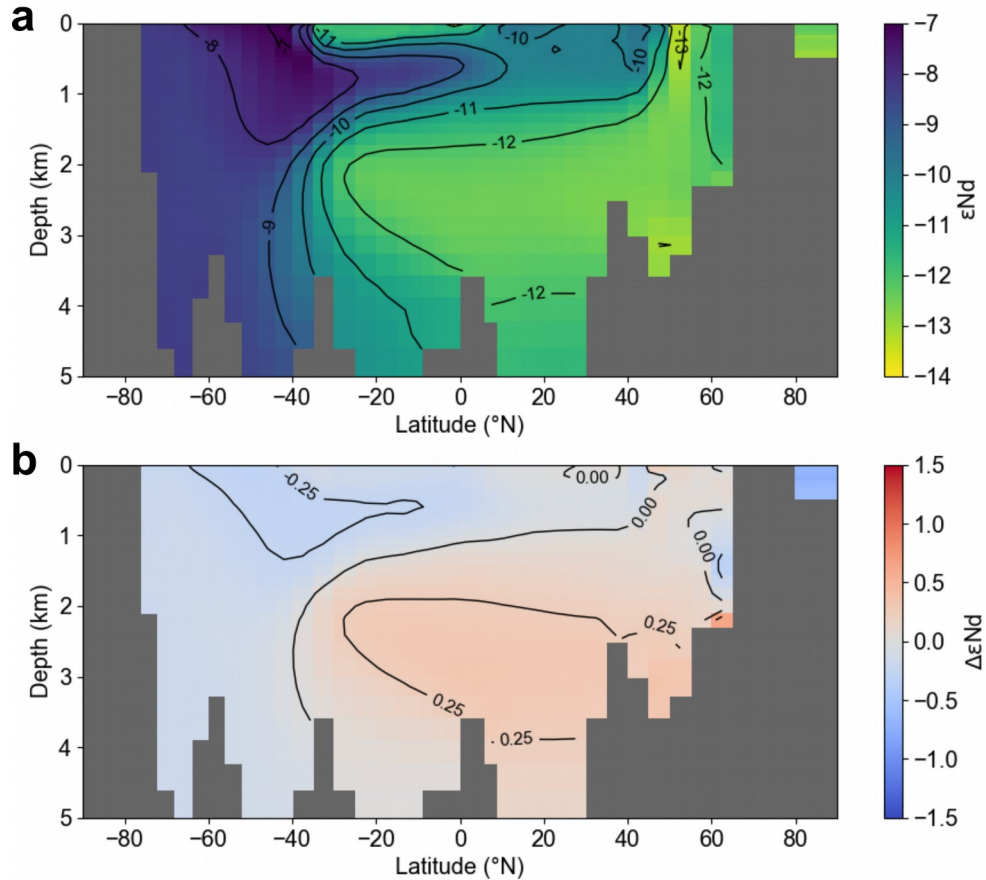
Figure S1: (a) Nd isotope distribution along the meridional section at 31.5°W with the benthic Nd flux scaling α_{bs} globally set to 1. All other parameters were kept constant. (b) Difference of panel a minus the control run (Figure 4b).

Further, we explored a second benthic Nd flux scaling distribution derived from global coretop – bottom water offsets (Figure S2). This distribution is based on the hypothesis that a potential benthic Nd flux not only influences the bottom water but also the pore-water and hence the authigenic sedimentary phase. Since Nd concentrations in pore-waters are two to three orders of magnitude larger than in bottom waters, a benthic flux would have a substantially larger impact on the authigenic phase than on bottom water εNd, thus producing a coretop – bottom water offset. This coretop – bottom water offset is then used as a measure for the benthic flux (Figure S2). However, it is not only dependent on the strength of the benthic flux but also the bottom water advection rate and the absolute difference in εNd between the detrital and authigenic phase (i.e. the smaller the difference between detrital and authigenic phase the smaller a potential offset between coretop (authigenic) and bottom waters, independent of the benthic flux). Hence, this approach comes with additional uncertainties. Moreover, the reported benthic Nd fluxes in the Cape Basin (Rahlf et al., 2020) and the North Pacific (Yu, 2019) are not represented in this approach. Overall, the differences between the Atlantic Nd

isotope distributions obtained with the different benthic flux scaling approaches (Figure 3d versus Figure S2) are close to zero (Figure S3). This is not surprising, considering that the dominating feature in both approaches is the strongly elevated benthic flux in the northern North Atlantic. However, the Pacific is too unradiogenic in this second approach (Figure S2), since the highly radiogenic Nd source in the North Pacific is missing.
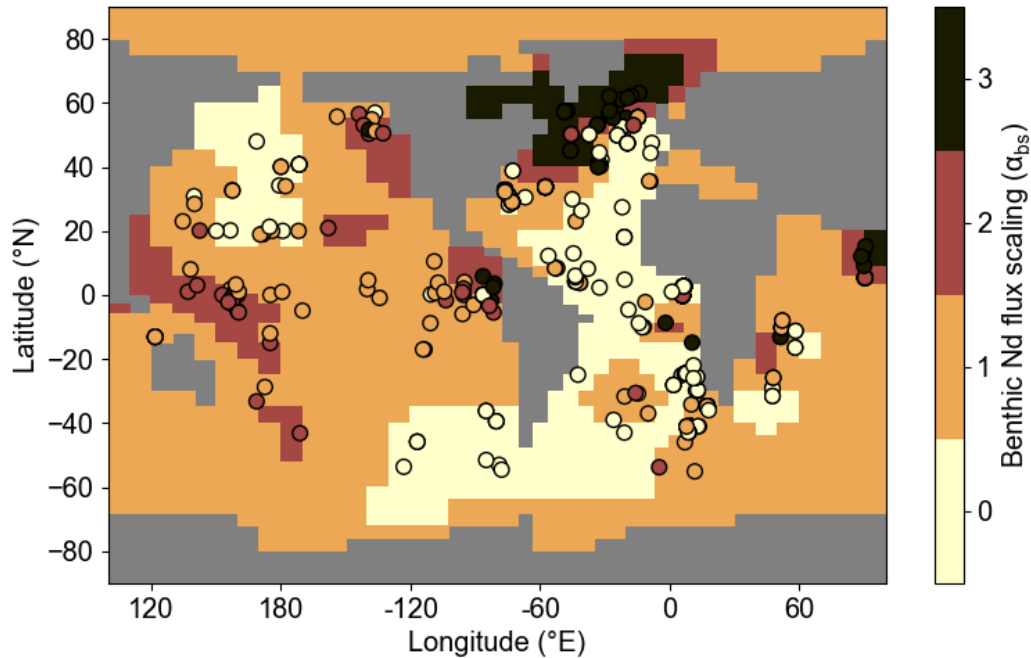

Figure S2: Alternative approach for the benthic Nd flux scaling based on coretop – bottom water offsets. Coretop – bottom water offsets are taken from Tachikawa et al. (2017) (circles) and are normalized to values between 0 and 3 to represent the benthic flux scaling. Interpolation of the data was performed with a multi-level B-spline approximation. Note that in contrast to the scaling distribution used for the control run, here also absent benthic fluxes ($\alpha_{bs} = 0$) are possible.
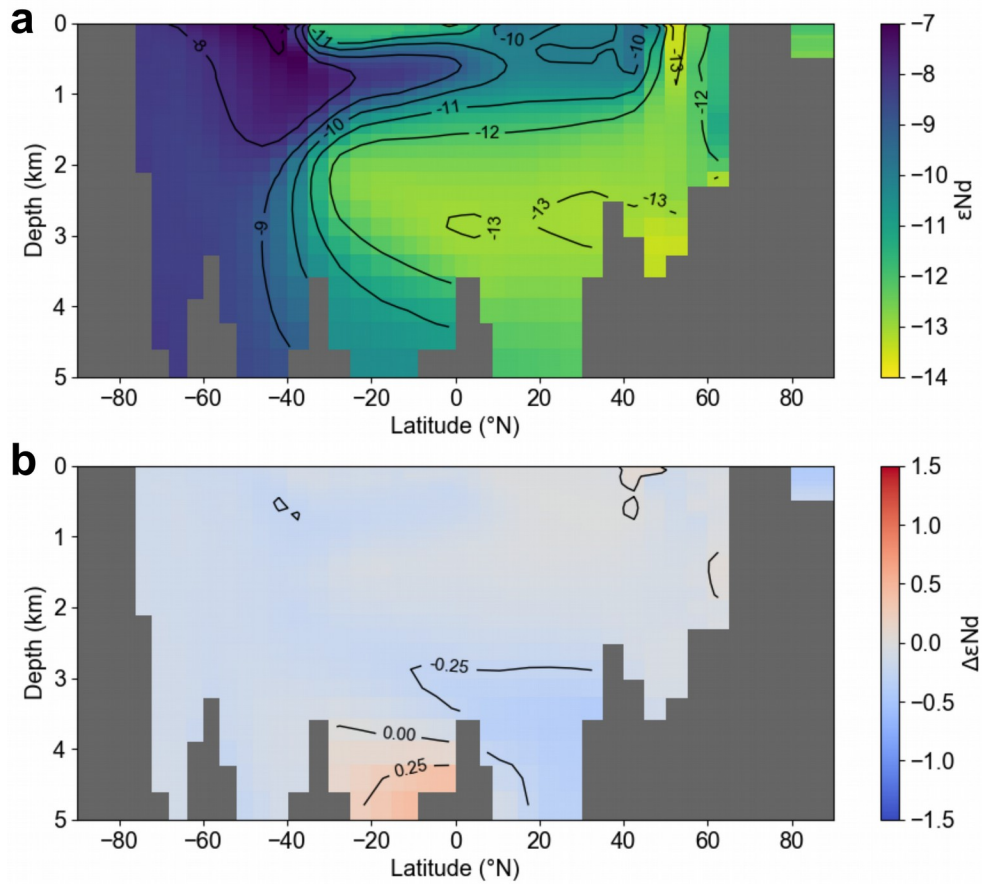
Figure S3: (a) Nd isotope distribution along the meridional section at 31.5°W with the benthic Nd flux scaling distribution as depicted in Figure S2. All other parameters were kept constant. (b) Difference of panel a minus the control run (Figure 4b).

Table S3: Model-data misfits (Mean Absolute Error: MAE) for control simulations compared to the updated NEOSYMPA database.

	[Nd]$_d$ (pmol/kg)	**εNd**
All water depths	6.5 (n = 2045)	1.54 (n = 1792)
250-2000 m	5.7 (n = 711)	1.43 (n = 824)
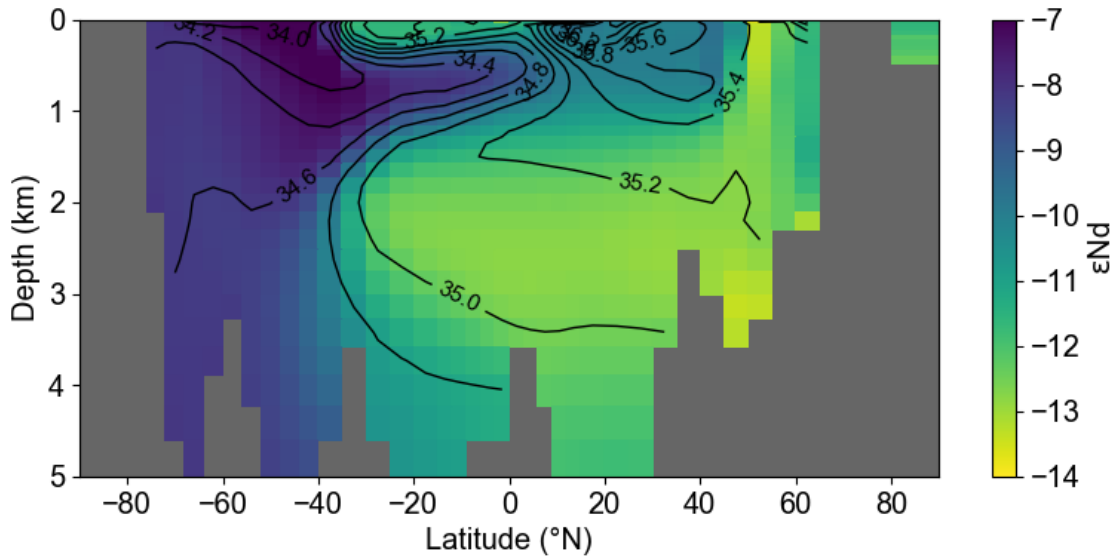
Figure S5: Same as Figure 4b, but with salinity contour lines in psu, indicating the quasi-conservative behavior of the Nd isotopic composition in the Bern3D model.
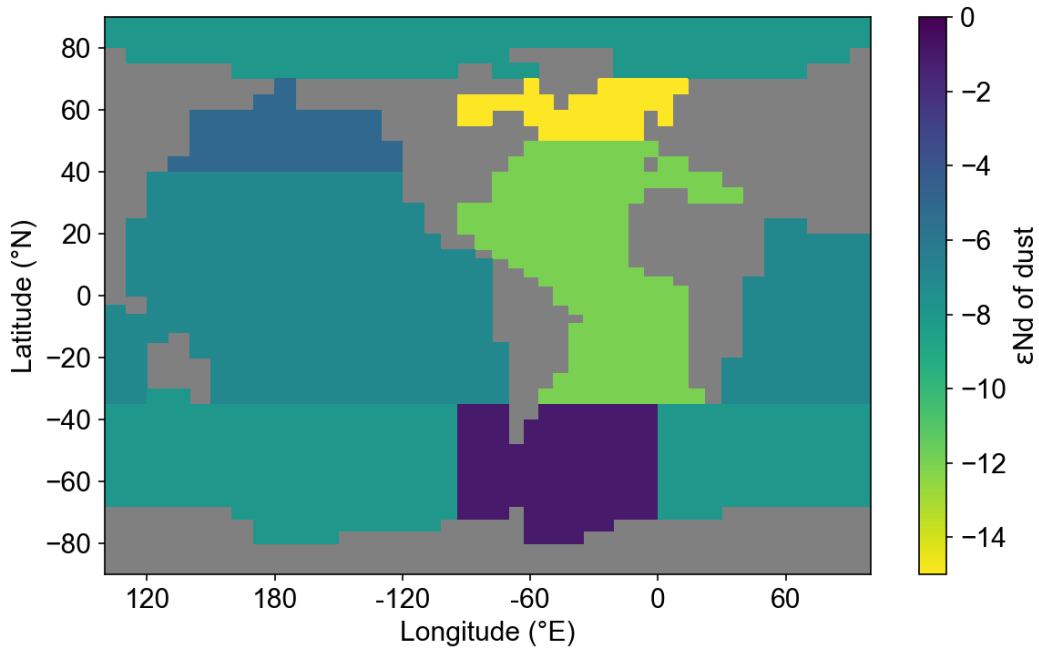
Figure S6: Prescribed Nd isotopic composition of dust after Tachikawa et al. (2003).
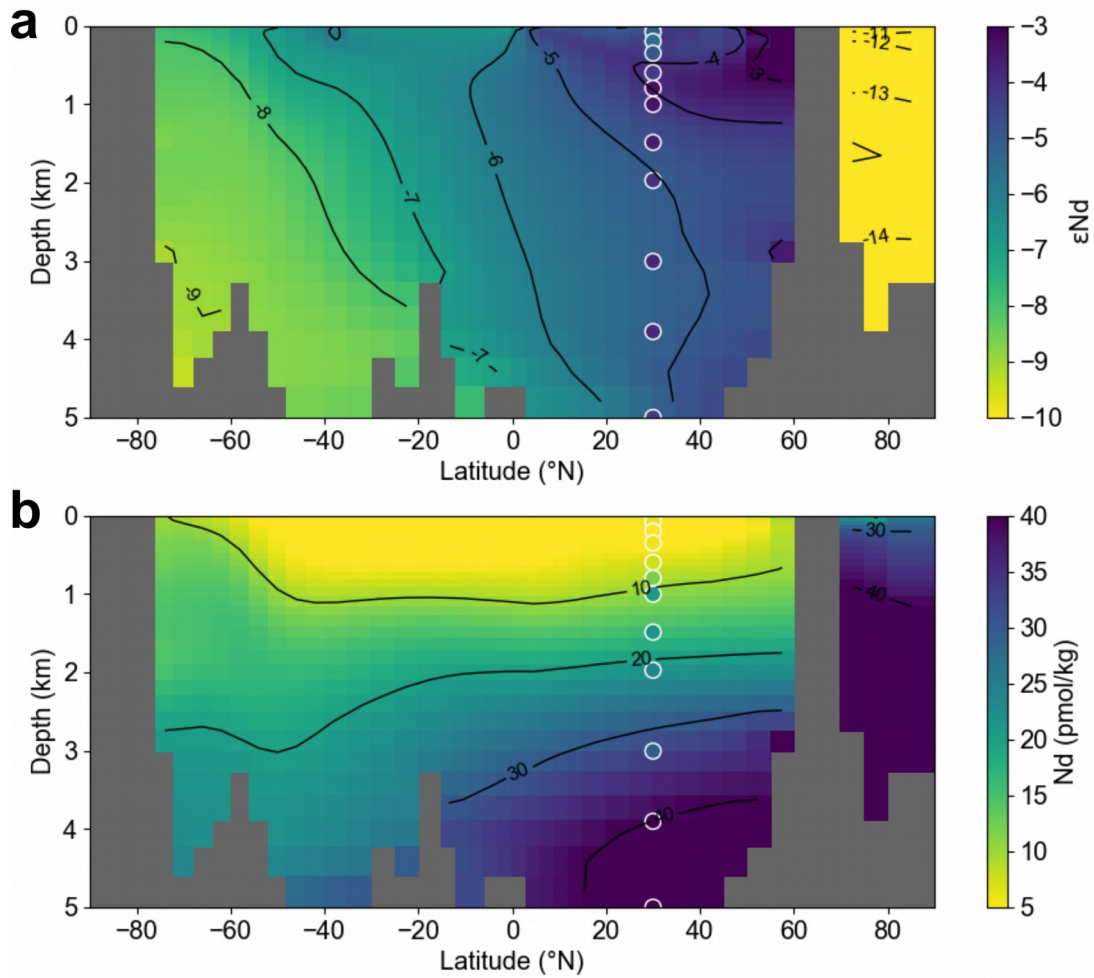
Figure S7: Meridional sections of the Pacific along 145°W for the control run. (a) Nd isotopic composition and (b) dissolved Nd concentration. Circles depict εNd and Nd concentrations of seawater station BO-3 (30°N, 160°W; Amakawa et al., 2009)
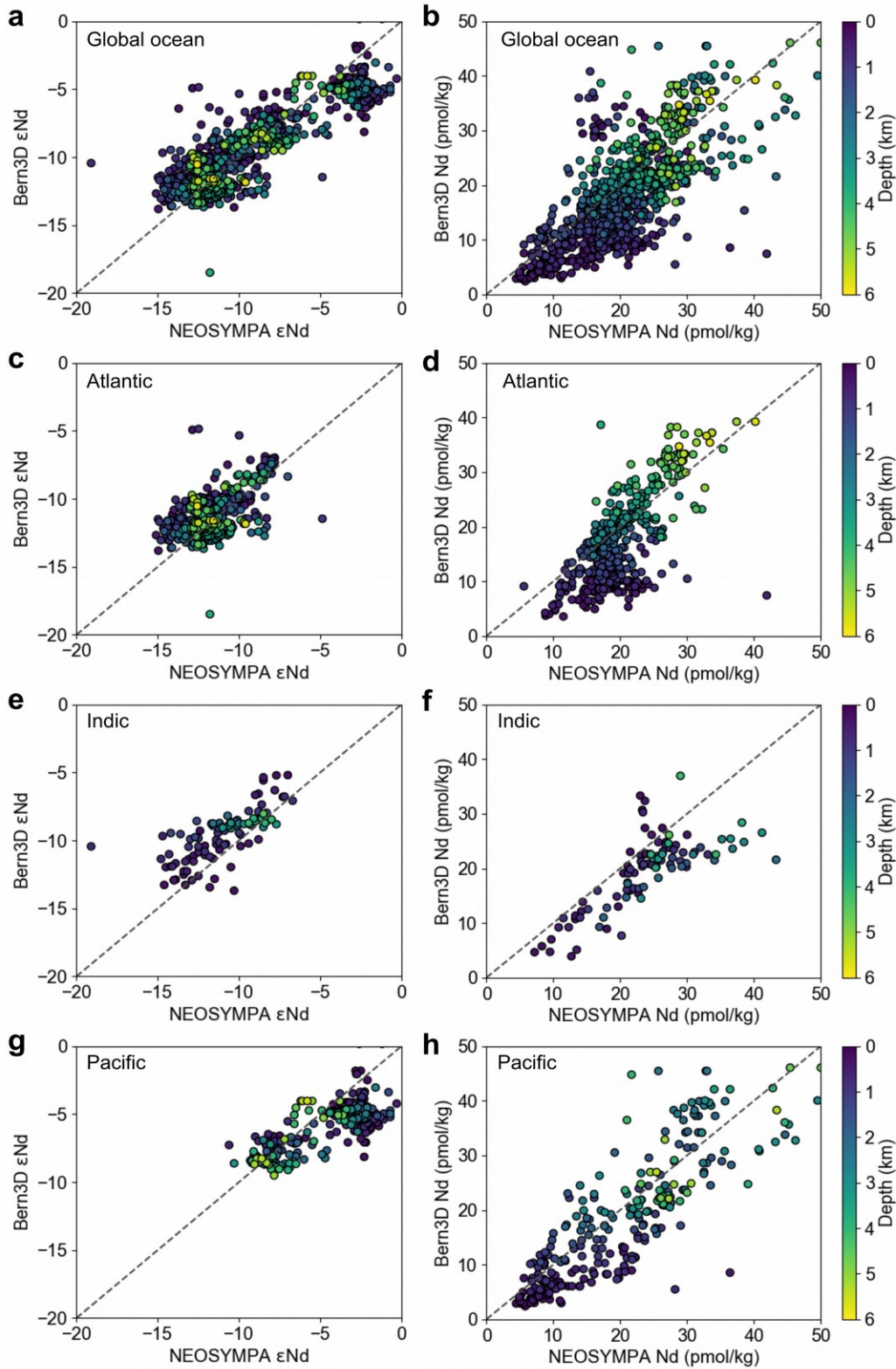
Figure S8: Cross-plots of εNd (left) and Nd concentration (right) of observational data of the NEOSYMPA database (Tachikawa et al., 2017) versus the Bern3D output of the control run. For each station, the value of the closest Bern3D grid cell is taken.

(a,b) Global ocean, (c,d) Atlantic, (e,f) Indic, (g,h) and Pacific. Stations shallower than 250 m are not considered here as described in the main text. The Mean Absolute Errors (MAE) are noted in the main text and for all data including the uppermost 250 m given in Table S3.
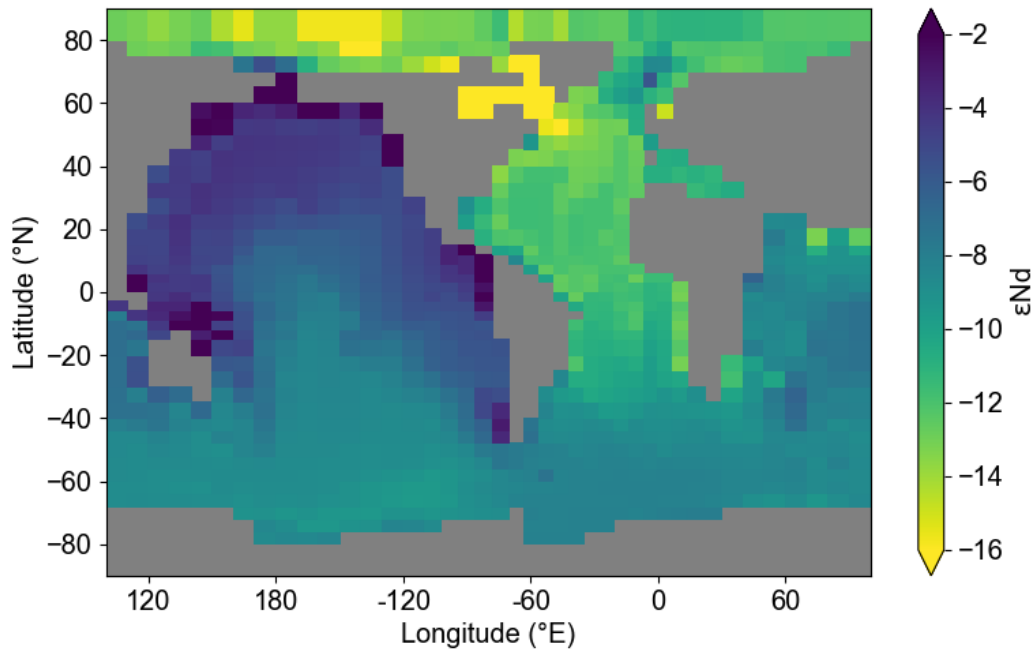

Figure S9: Global map of dissolved Nd isotopic signatures at the bottommost grid cell simulated for the control run. εNd signatures in the Baffin Bay go down to less than -20.
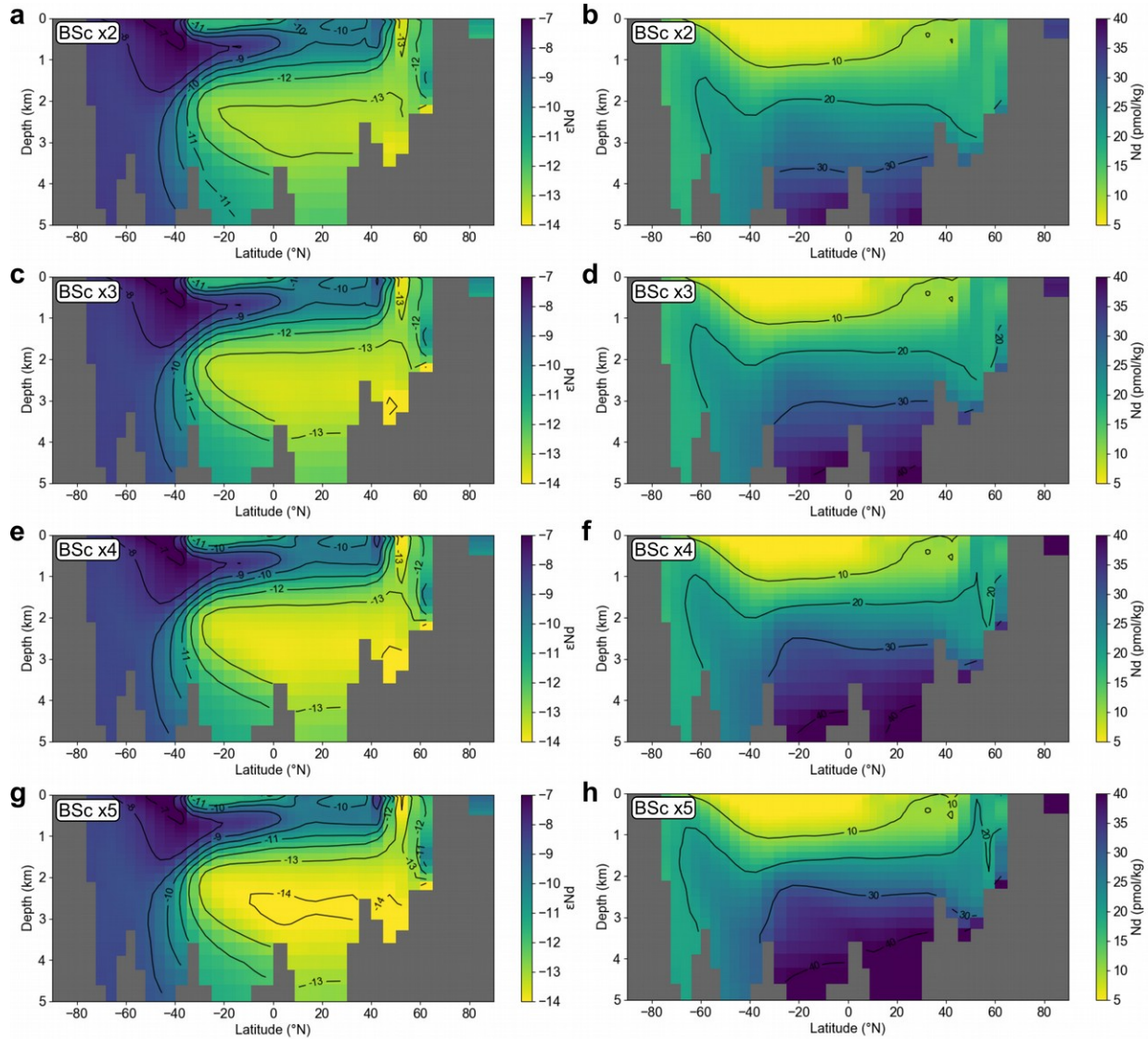
Figure S10: εNd and Nd concentrations of the sensitivity tests of the meridional section at 31.5°W. (a,b) Doubling, (c,d) tripling, (e,f) quadrupling, and (g,h) quintupling of the benthic Nd flux scaling in the North Atlantic grid cells with base scaling factors >1 (orange and black areas in Figure 3d). Figure 5 corresponds to the panels (a,c,e,g) minus the control run (Figure 4b).
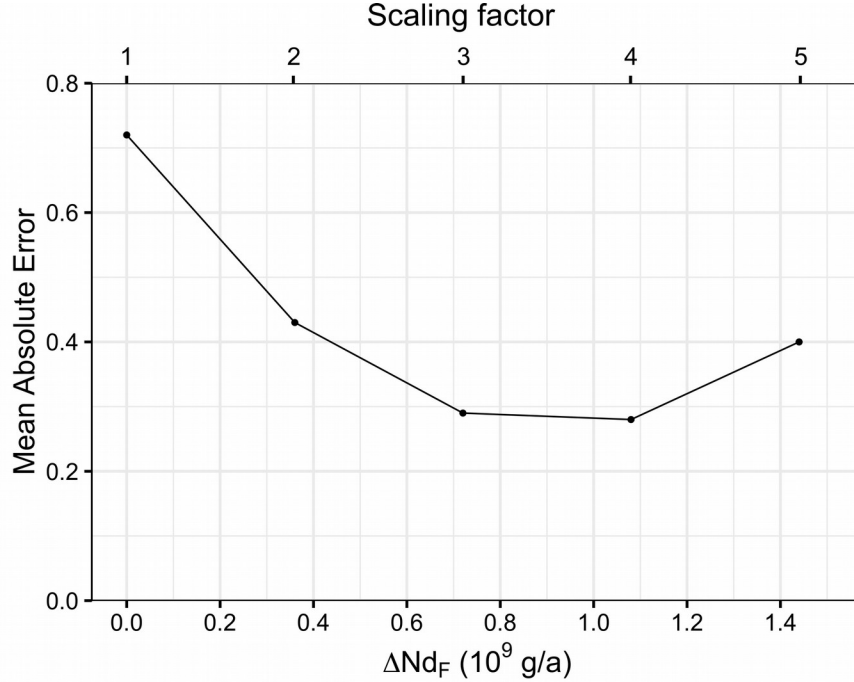
Figure S11: Mean Absolute Error (MAE) of the early Holocene εNd anomaly in the Atlantic versus the additional benthic Nd flux applied to the northern North Atlantic (orange and black areas in Figure 3d) in the sensitivity tests. Upper x-axis depicts the additional benthic flux in terms of scaling factors as also described in the main text (section 3.1). The MAE is minimized at a scaling factor of 3 or 4.

Sediment dissolution rate corresponding to benthic flux scaling factors

We estimate the detrital sediment dissolution rates corresponding to the best fit benthic flux scaling factor between 3 and 4 (cf. Figure S11). For this, we assume a mean particulate Nd concentration ($[Nd]_p$) of 27 ppm (Rudnick and Gao, 2003), 2 cm/ka average sedimentation rate (S), and an area (A) of 1×10^7 km^2 for the northern North Atlantic with elevated benthic Nd fluxes. For the mean sediment density (D) we assume a value of 2.7 g/cm^3 and a detrital sediment fraction (f_D) of 50%. From this we get a total Nd flux F_{Nd} of:

$$F_{Nd} = V_{Nd, detrital} \cdot [Nd]_p = A \cdot S \cdot D \cdot f_D \cdot [Nd]_p \approx 1.46 \times 10^{10}\ g/yr$$

This conservative estimate for the annual particulate Nd flux of the northern North Atlantic yields total sediment dissolution rates in the range of 4.9% to 7.4% for the benthic flux scalings of 3 to 4 corresponding to additional Nd fluxes between 0.72 and 1.08×10^9 g/yr. These sediment dissolution rates are upper limits, since we neglect the possibility that less radiogenic material could have contributed to the early Holocene anomaly, which would lower the required additional Nd flux and hence the sediment dissolution rates.

References

Amakawa, H., Sasaki, K., & Ebihara, M. (2009). Nd isotopic composition in the central North Pacific. Geochimica et Cosmochimica Acta, 73(16), 4705–4719. https://doi.org/10.1016/j.gca.2009.05.058

Blaser, P., Gutjahr, M., Pöppelmeier, F., Frank, M., Kaboth-Bahr, S., Lippold, J. (2020). Labrador Sea bottom water provenance and REE exchange over the past 35,000 years. *Earth and Planetary Science Letters*, 542, 116299.

Doney, S. C., Lindsay, K., Fung, I., & John, J. (2006). Natural variability in a stable, 1000-yr global coupled climate-carbon cycle simulation. *Journal of Climate*, *19*(13), 3033–3054. https://doi.org/10.1175/JCLI3783.1

Edwards, N. R., Willmott, A. J., & Killworth, P. D. (1998). On the role of topography and wind stress on the stability of the thermohaline circulation. *Journal of Physical Oceanography*, *28*(5), 756–778. https://doi.org/10.1175/1520-0485(1998)028<0756:OTROTA>2.0.CO;2

Griffies, S. M. (1998). The Gent-McWilliams skew flux. *Journal of Physical Oceanography*, *28*(5), 831–841. https://doi.org/10.1175/1520-0485(1998)028<0831:TGMSF>2.0.CO;2

Howe, J. N. W., Piotrowski, A. M., Hu, R., & Bory, A. (2017). Reconstruction of east–west deep water exchange in the low latitude Atlantic Ocean over the past 25,000 years. *Earth and Planetary Science Letters*, *458*, 327–336. https://doi.org/10.1016/j.epsl.2016.10.048

Howe, J. N. W., Piotrowski, A. M., Oppo, D. W., Huang, K. F., Mulitza, S., Chiessi, C. M., & Blusztajn, J. (2016a). Antarctic intermediate water circulation in the South Atlantic over the past 25,000 years. *Paleoceanography, 31(10)*, 1302–1314. https://doi.org/10.1002/2016PA002975

Howe, J. N. W., Piotrowski, A. M., & Rennie, V. C. F. (2016b). Abyssal origin for the early Holocene pulse of unradiogenic neodymium isotopes in Atlantic seawater. *Geology*, *44*(10), 831–834. https://doi.org/10.1130/G38155.1

Kalnay, E., Kanamitsu, M., Kistler, R., Collins, W., Deaven, D., Gandin, L., Iredell, M., Saha, S., White, G., Wollen, J., Zhu, Y., Chelliah, M., Ebisuzaki, W., Higgins, W., Janowiak, J., Mo, K. C., Ropelewski, C., Wang, J., Leetmaa, A., … Joseph, D. (1996). The NCEP NCAR 40-Year Reanalysis Project. *Bulletin of the American Meteorological Society, 77(3)*, 437–472. https://doi.org/10.1175/1520-0477(1996)077<0437:TNYRP>2.0.CO;2

Martin, J. H., Knauer, G. A., Karl, D. M., & Broenkow, W. W. (1987). VERTEX: carbon cycling in the northeast Pacific. *Deep Sea Research Part A, Oceanographic*

Research Papers, *34*(2), 267–285. https://doi.org/10.1016/0198-0149(87)90086-0

Lippold, J., Gutjahr, M., Blaser, P., Christner, E., de Carvalho Ferreira, M. L., Mulitza, S., Christl, M., Wombacher, F., Böhm, E., Antz, B., Cartapanis, O., Vogel, H., & Jaccard, S. L. (2016). Deep water provenance and dynamics of the (de)glacial Atlantic meridional overturning circulation. *Earth and Planetary Science Letters*, *445*, 68–78. https://doi.org/10.1016/j.epsl.2016.04.013

Luo, C., Mahowald, N. M., & del Corral, J. (2003). Sensitivity study of meteorological parameters on mineral aerosol mobilization, transport, and distribution. Journal of Geophysical Research D: Atmospheres, 108(15). https://doi.org/10.1029/2003jd003483

Mahowald, N. M., Muhs, D. R., Levis, S., Rasch, P. J., Yoshioka, M., Zender, C. S., & Luo, C. (2006). Change in atmospheric mineral aerosols in response to climate: Last glacial period, preindustrial, modern, and doubled carbon dioxide climates. Journal of Geophysical Research Atmospheres, 111(10). https://doi.org/10.1029/2005JD006653

Müller, S. A., Joos, F., Edwards, N. R., & Stocker, T. F. (2006). Water mass distribution and ventilation time scales in a cost-efficient, three dimensional ocean model. *Journal of Climate*, *19*(21), 5479–5499. https://doi.org/10.1175/JCLI3911.1

Parekh, P., Joos, F., & Müller, S. A. (2008). A modeling assessment of the interplay between aeolian iron fluxes and iron-binding ligands in controlling carbon dioxide fluctuations during Antarctic warm events. *Paleoceanography*, *23*(4), 1–14. https://doi.org/10.1029/2007PA001531

Poggemann, D. W., Nürnberg, D., Hathorne, E. C., Frank, M., Rath, W., Reißig, S., & Bahr, A. (2018). Deglacial Heat Uptake by the Southern Ocean and Rapid Northward Redistribution Via Antarctic Intermediate Water. *Paleoceanography and Paleoclimatology, 33(11)*, 1292–1305. https://doi.org/10.1029/2017PA003284

Pöppelmeier, F., Blaser, P., Gutjahr, M., Süfke, F., Thornalley, D. J. R., Grützner, J., Jakob, K. A., Link, J. M., Szidat, S., & Lippold, J. (2019). Influence of Ocean Circulation and Benthic Exchange on Deep Northwest Atlantic Nd Isotope Records During the Past 30,000 Years. *Geochemistry, Geophysics, Geosystems*, *20*(9), 4457–4469. https://doi.org/10.1029/2019GC008271

Pöppelmeier, F., Gutjahr, M., Blaser, P., Oppo, D. W., Jaccard, S. L., Regelous, M., Huang, K., Süfke, F., & Lippold, J. (2020). Water mass gradients of the mid-depth Southwest Atlantic during the past 25,000 years. *Earth and Planetary Science Letters*, *531,* 115963. https://doi.org/10.1016/j.epsl.2019.115963

Rempfer, J., Stocker, T. F., Joos, F., Dutay, J. C., & Siddall, M. (2011). Modelling Nd-isotopes with a coarse resolution ocean circulation model: Sensitivities to model parameters and source/sink distributions. *Geochimica et Cosmochimica Acta*, *75*(20), 5927–5950. https://doi.org/10.1016/j.gca.2011.07.044

Rempfer, J., Stocker, T. F., Joos, F., & Dutay, J. C. (2012). On the relationship between Nd isotopic composition and ocean overturning circulation in idealized freshwater discharge events. Paleoceanography, 27(3), 1–24. https://doi.org/10.1029/2012PA002312

Rudnick, R. L. & Gao, S. Composition of the Continental Crust. In Treatise on Geochemistry; Elsevier, 2003; Vol. 3, pp 1–64. https://doi.org/10.1016/B0-08-043751-6/03016-4

Schlitzer, R., Anderson, R. F., Masferrer, E., Lohan, M., Daniels, C., Dehairs, F., Deng, F., Thi, H., & Duggan, B. (2018). *The GEOTRACES Intermediate Data Product 2017*. *Chemical Geology 493*, 210-223. https://doi.org/10.1016/j.chemgeo.2018.05.040

Skinner, L. C., Scrivner, A. E., Vance, D., Barker, S., Fallon, S., & Waelbroeck, C. (2013). North atlantic versus southern ocean contributions to a deglacial surge in deep ocean ventilation. *Geology, 41(6)*, 667–670. https://doi.org/10.1130/G34133.1

Tachikawa, K., Athias, V., & Jeandel, C. (2003). Neodymium budget in the modern ocean and paleo-oceanographic implications. Journal of Geophysical Research, 108(C8), 3254. https://doi.org/10.1029/1999JC000285

Tachikawa, K., Arsouze, T., Bayon, G., Bory, A., Colin, C., Dutay, J. C., Frank, N., Giraud, X., Gourlan, A. T., Jeandel, C., Lacan, F., Meynadier, L., Montagna, P., Piotrowski, A. M., Plancherel, Y., Pucéat, E., Roy-Barman, M., & Waelbroeck, C. (2017). The large-scale evolution of neodymium isotopic composition in the global modern and Holocene ocean revealed from seawater and archive data. *Chemical Geology*, *457*, 131–148. https://doi.org/10.1016/j.chemgeo.2017.03.018

Tschumi, T., Joos, F., & Parekh, P. (2008). How important are Southern Hemisphere wind changes for low glacial carbon dioxide? A model study. *Paleoceanography*, *23*(4), 1–20. https://doi.org/10.1029/2008PA001592

Wei, R., Abouchami, W., Zahn, R., & Masque, P. (2016). Deep circulation changes in the South Atlantic since the Last Glacial Maximum from Nd isotope and multi-proxy records. *Earth and Planetary Science Letters, 434*, 18–29. https://doi.org/10.1016/j.epsl.2015.11.001

Wu, Y. (2019). Investigating the Applications of Neodymium Isotopic Compositions and Rare Earth Elements as Water Mass Tracers in the South Atlantic and North Pacific. *PhD Thesis*, Columbia University. https://doi.org/10.7916/d8-kstx-xg38

Zhao, N., Oppo, D. W., Huang, K. F., Howe, J. N. W., Blusztajn, J., & Keigwin, L. D. (2019). Glacial–interglacial Nd isotope variability of North Atlantic Deep Water modulated by North American ice sheet. *Nature Communications*, *10*(1), 1–10. https://doi.org/10.1038/s41467-019-13707-z